

Critical Tunneling Currents in Quantum Hall Superfluids: Pseudospin-Transfer Torque Theory

Jung-Jung Su^{1,2} and Allan H. MacDonald¹

¹ *Department of Physics, The University of Texas at Austin, Austin, TX 78712, USA and*

² *Theoretical Division, Los Alamos National Laboratory, Los Alamos, New Mexico 87545, USA*

(Dated: February 22, 2024)

At total filling factor $\nu = 1$ quantum Hall bilayers can have an ordered ground state with spontaneous interlayer phase coherence. The ordered state is signaled experimentally by dramatically enhanced interlayer tunnel conductances at low bias voltages; at larger bias voltages inter-layer currents are similar to those of the disordered state. We associate this change in behavior with the existence of a critical current beyond which static inter-layer phase differences cannot be maintained, and examine the dependence of this critical current on sample geometry, phase stiffness, and the coherent tunneling energy density. Our analysis is based in part on analogies between coherent bilayer behavior and spin-transfer torque physics in metallic ferromagnets. Comparison with recent experiments suggests that disorder can dramatically suppress critical currents.

PACS numbers:

I. INTRODUCTION

At Landau level filling factor $\nu = 1$ bilayer two-dimensional electron systems in the quantum Hall regime can have broken symmetry ground states^{1–4} with spontaneous inter-layer phase coherence. These ordered states can be viewed as excitonic superfluids,^{5,6} or as XY pseudospin ferromagnets⁷ in which the pseudospin is formed from the two-valued *which layer* quantum degree of freedom. The most robust experimental signature of these states, a vastly enhanced inter-layer tunnel conductance^{8–11} at small bias voltages, is still poorly understood from a quantitative point of view.

Two types of ideas, which differ most essentially in how the bias voltage is introduced in the theory, have been explored in an effort to understand the height and width of the tunnel conductance peak. In one approach^{12–15} the bias voltage is introduced as an effective magnetic field, uniform across the bilayer, which induces pseudospin precession around the \hat{z} axis, driving the interlayer phase difference at a steady rate and inducing a purely oscillating inter-layer current. When the microscopic inter-layer tunneling amplitude is treated as a perturbation, thermal and disorder fluctuations of the condensate are then responsible for a finite dc conductance peak. We refer to this type of theory below as the weak-coupling theory of the tunneling anomaly. Weak-coupling theories predict^{12–15} splitting of the zero voltage tunnel conductance peak into separate finite voltage peaks in the presence of a magnetic field component parallel to the two-dimensional layers, an effect that is not¹⁶ seen experimentally. The second type of transport theory^{17–21} is formulated in terms of local chemical potentials of fermionic quasiparticles which may be altered by the ordered state condensate but are still responsible for charge conduction. In this type of theory the tunnel conductance is finite even in the absence of disorder and thermal fluctuations because charge has to be driven between normal-metal source and drain contacts. The resistance

generally depends^{18,21} on how the fermionic degrees of freedom which carry charge between leads are influenced by order parameter and disorder configurations and cannot be described in terms of condensate dynamics alone. In the second approach the width in voltage of the conductance peak is simply equal to the product of this resistance and the maximum current between source and drain at which the order parameter can maintain a time-independent steady-state value.

In this article we expand on the second type of theory of the conductance peak, using pseudospin-transfer torque ideas^{22,23} borrowed from recent ferromagnetic-metal spintronics literature to model the influence of the transport current on the pseudospin magnetization. We find that the critical current depends in general on details of the sample geometry and on how disorder and localization physics influence transport inside the system. Generally speaking however, the critical current is proportional to system area and to the inter-layer tunneling amplitude when the condensate's Josephson length is larger than the system perimeter, and proportional to the system perimeter and to the square root of the inter-layer tunneling amplitude when it is shorter.

Our paper is organized as follows. In Section II we introduce the pseudospin-transfer torque theory of order-parameter dynamics in a bilayer quantum Hall ferromagnet. We use this theory in Section III to discuss critical current values from a qualitative point of view. In Section IV we report on a series of numerical studies which take into account the two-dimensional nature of the systems of interest and the edge dominated current-paths typical of strong magnetic fields. The pseudospin transfer torque theory enables us to assess the influence of sample geometry on critical currents. Finally in Section V we discuss the significance of our findings in relation to recent experiments. We find that experimental critical currents are several orders of magnitude smaller than theoretical ones and argue that vortex-like disorder-induced pseudospin textures must be largely responsible for this discrepancy.

We propose new experimental studies which can test our ideas and thereby achieve progress toward a quantitative theory of the spontaneous coherence tunneling anomaly.

II. PSEUDOSPIN MAGNETISM AND THE LANDAU-LIFSHITZ-SLONCZEWSKI EQUATION

In the lattice model²⁴ of $\nu = 1$ bilayer systems, the local *which* layer degree of freedom can be expressed as a pseudospin defined by the operator

$$\vec{S}_i = \frac{1}{2} \sum_{\sigma, \sigma'} a_{i, \sigma}^\dagger \vec{\tau}_{\sigma, \sigma'} a_{i, \sigma'} \quad (1)$$

where i is the site index, σ is the layer index and $\vec{\tau}$ is the Pauli matrix vector. The pseudospin Hamiltonian has the form²⁴

$$H_{\text{int}} = \frac{1}{2} \sum_{i,j} (2H_{i,j} - F_{i,j}^S) S_i^z S_j^z - F_{i,j}^D (S_i^x S_j^x + S_i^y S_j^y) \quad (2)$$

where $H_{i,j} = \langle i, \sigma; j, \sigma' | V_{\text{col}} | i, \sigma; j, \sigma' \rangle$ is the direct Coulomb interaction associated with the \hat{z} pseudospin component (*i.e.* with charge transfer between layers), $F_{i,j}^S = \langle i, \sigma; j, \sigma | V_{\text{col}} | i, \sigma; j, \sigma \rangle$, is the exchange interaction between orbitals in the same layer and $F_{i,j}^D = \langle i, \sigma; j, \bar{\sigma} | V_{\text{col}} | i, \sigma; j, \bar{\sigma} \rangle$ is the exchange interaction between orbitals located in different layers. Since $H_{i,j}$ is generally larger than $F_{i,j}^S$, the classical ground state is an easy-plane pseudospin ferromagnet with a hard \hat{z} axis. In the limit of smooth textures the pseudospin energy functional has the form⁷

$$E[\vec{m}] = \int d^2r \left\{ \beta (m_z)^2 + \frac{1}{2} \rho_s \left[|\vec{\nabla} m_x|^2 + |\vec{\nabla} m_y|^2 \right] - \frac{1}{2} \Delta_t n m_x \right\} \quad (3)$$

where $\vec{m} = \{m_x, m_y, m_z\}$ is the local pseudospin direction. The parameters which appear in this expression are the anisotropy parameter $\beta > 0$, the pseudospin stiffness (or equivalently the exciton superfluid density) ρ_s , the splitting between symmetric and antisymmetric single-particle bilayer states due to interlayer tunneling Δ_t , and the pseudospin density n .

The mean-field-theory pseudospin ferromagnet¹ consists of a full Landau level of electrons in identical phase coherent bilayer states. It follows that the mean-field-theory pseudospin density n is equal to the full Landau level density, $(2\pi l^2)^{-1}$. (Here $l = (\hbar c/eB)^{1/2}$, where B is the magnetic field strength, is the magnetic length.) Mean-field-theory can also be used⁷ to find explicit expressions for ρ_s and β . In practice the values of these three parameters are modified²⁵ by quantum and thermal fluctuations. The fourth parameter Δ_t is exponentially sensitive to the tunnel barrier between layers. Parameters values can also be influenced by disorder on length scales

shorter than those on which this coarse-grained continuum theory is applied; disorder on longer length scales would have to be treated explicitly as we mention in the discussion section. The upshot is that the numerical values of the parameters in Eq.(3) are usually not accurately known and likely vary substantially from sample to sample. It is worth noting that n must vanish at finite temperatures when $\Delta_t \rightarrow 0$ since two-dimensional systems cannot support spontaneous long-range phase order. Among all continuum model parameters the value of ρ_s , which is typically $\sim 10^{-4}$ eV, is likely the most reliably known.

Since the *which layer* pseudospin and the true electron spin have identical quantum mechanical descriptions, we can borrow from the ferromagnetic metal spintronics literature^{22,23} and use the Landau-Lifshitz-Slonczewski (LLS) equation to describe how the semiclassical pseudospin dynamics is influenced by a transport current:

$$\frac{d\vec{m}}{dt} = \vec{m} \times \vec{H}_{\text{eff}} - \frac{(\vec{j} \cdot \partial \vec{\tau}) \vec{m}}{n} - \alpha \left(\vec{m} \times \frac{d\vec{m}}{dt} \right). \quad (4)$$

(\vec{j} is the number current density for electrons.) The second term on the right-hand-side of Eq.(4) captures the transport current effect. Its role in these equations is similar to the role played by the leads in the pioneering analysis of coherent bilayer tunneling by Wen and Zee¹⁷ who argued that a term should be added to the global condensate equation of motion to account for the contribution of transport currents to the difference in population between top and bottom layers. Eq.(4) describes how a transport current alters the condensate equation of motion locally. Its justification for the bilayer quantum Hall case is discussed in more detail below. The essential validity of this expression has been verified by countless experiments. In the first term on the right hand side

$$\vec{H}_{\text{eff}} = (2/\hbar n)(\delta E[\vec{m}]/\delta \vec{m}) \quad (5)$$

describes precessional pseudospin dynamics in an effective magnetic field which is defined by the energy functional. The third term accounts for damping of the collective motion due to coupling to its environment, in the present case the Fermi sea of quasiparticles. The damping term in Eq.(4) has the standard isotropic form used in the magnetism literature. A microscopic theory²⁶ of damping in quantum Hall bilayers makes it clear that the damping is actually quite anisotropic. We return to this point below.

Magnetic order in the metallic ferromagnets to which this equation is normally applied is extremely robust, justifying the assumption that the spin-density magnitude is essentially unchanged even when the system is driven from equilibrium by a transport current. The only relevant degree of freedom is the spin-density direction, whose dynamics is described by Eq.(4). We expect that the pseudospin transfer torque description of bilayer quantum Hall systems will be most reliable when the order is most firmly established, that is far away from the

phase boundary²⁷ that separates ordered and disordered states.

The transport-current (Slonczewski²³) term in Eq.(4) can be understood in several different ways. In the spintronics literature this term is normally motivated by an appeal to total spin conservation and referred to as the spin-transfer torque. The idea is that when a ferromagnet's spin-polarized quasiparticles carry a transport current through a spatial region with a non-collinear magnetization, they violate spin-conservation. The collective magnetization must therefore compensate by rotating at a constant rate which is proportional to the fermion drift velocity. The form we use for the pseudospin transfer torque assumes that each component of the pseudospin current is locally equal to the number current times the corresponding pseudospin direction cosine. This property does not hold locally in a microscopic theory, but is expected to be valid in the smooth pseudospin texture limit we address. (In metals an additional phenomenological factor is required to account for the difference in drift velocity between majority and minority spin electrons.)

Since pseudospin is not conserved in bilayer quantum Hall systems, as we can see from Eq.(2) or Eq.(3), this argument does not apply directly. If we appeal to a mean-field description of the pseudospin ferromagnet, however, we can obtain the same result by the following argument. Mean-field quasiparticles satisfy a single-particle Hamiltonian for a particle in a magnetic field which experiences both a scalar potential, and a pseudospin-dependent potential that can be interpreted as a pseudospin effective magnetic field. Following standard textbook derivations it is possible²⁸ to derive an expression for the time-dependence of the contribution of a single quasiparticle to any component of the pseudospin density. The expression contains a pseudospin precession term and an additional term which is the divergence of the current of that component of pseudospin. Summing over all quasiparticle states we obtain a precession term that depends on the configuration of the order parameter, and hence on the pseudospin-field to which it gives rise, even in the absence of a current. We obtain the additional current-driven term on the right-hand side of Eq.(4) when the pseudospin currents are non-zero and space dependent. The additional term in the equation of motion can also be viewed²⁹ as a consequence of an altered relationship between pseudospin-dependent effective magnetic field and pseudospin polarization direction for quasiparticles that carry a current. Eq.(4) should in principle also include a current related damping term³⁰ which we ignore in the present paper.

When quantum Hall bilayer pseudospin ferromagnets are tilted far from their easy plane, order tends³¹ to be destroyed. For that reason we are often most interested in the limit in which m_z is much less than 1. It is therefore convenient to express the pseudospin direction in terms of the azimuthal angle ϕ , which is the inter-layer phase difference, and m_z which is proportional to the layer po-

larization. In terms of these variables the LLS equations take the form

$$\begin{aligned} \dot{m}_z &= \left\{ -\frac{2}{n\hbar} \rho_s m_\perp^2 \vec{\nabla}^2 \phi + \frac{\Delta_t}{\hbar} m_\perp \sin \phi \right\} \\ &\quad - \left(\vec{v}_{ps} \cdot \vec{\nabla} \right) m_z \Big\} + \alpha_z m_\perp^2 \dot{\phi} \\ \dot{\phi} &= m_z \left\{ \frac{2}{n\hbar} \rho_s \left(|\vec{\nabla} \phi|^2 + \frac{2}{m_\perp^4} |\vec{\nabla} m_z|^2 + \frac{2m_z}{m_\perp^2} \vec{\nabla}^2 m_z \right) \right. \\ &\quad \left. - \frac{4}{n\hbar} \beta - \frac{\Delta_t}{\hbar} \frac{1}{m_\perp} \cos \phi \right\} \\ &\quad - \left(\vec{v}_{ps} \cdot \vec{\nabla} \right) \phi \Big\} - \frac{\alpha_\phi}{m_\perp^2} \dot{m}_z. \end{aligned} \quad (6)$$

In Eq.(6) we have written \vec{j}/n , which has units of velocity, as the pseudospin velocity \vec{v}_{ps} .

These equations do not on their own provide a closed description of pseudospin dynamics in the presence of electrical bias potentials and need to be supplemented by a theory which specifies the spatial dependence of the pseudospin current. In general this quantity depends²¹ on the order parameter configuration as well as on the contact geometry and external current or voltage biases. The transport theory and the pseudospin dynamics theory are therefore not independent. In the present paper we study voltage biased Hall bars with source and drain leads at opposite ends, and with a variety of shapes and sizes. We assume, as a simplification, that the current distribution is defined by a local conductivity tensor with a large Hall angle. Given these simplifications, we are able to explicitly evaluate the maximum current at which time-independent order parameters are possible. Because collective tunneling no longer contributes strongly to the *dc* interlayer current when the inter-layer phase is time-dependent, the interlayer conductance mechanism changes qualitatively when this maximum current is exceeded. We therefore associate this current with the experimental critical current.

III. APPROXIMATE CRITICAL CURRENTS

In this section we discuss approximate upper bounds on the critical current which are helpful in interpreting the numerical results described in the following section. We use a simplified version of the static limit of the \dot{m}_z LLS equation (Eq.(6)) in which m_z is assumed to be small:

$$0 = -\frac{\rho_s}{\hbar} \vec{\nabla}^2 \phi + \frac{1}{2} \frac{\Delta_t n}{\hbar} \sin \phi - \frac{1}{2} \vec{j} \cdot \vec{\nabla} m_z. \quad (7)$$

The three terms on the right-hand side can be identified as contributions to the time-dependence of m_z (or equivalently of the exciton density) due respectively to the divergence of the exciton supercurrent, coherent condensate tunneling, and the divergence of the \hat{z} (layer

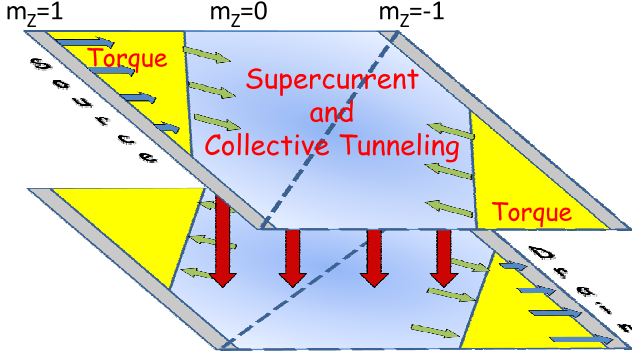


FIG. 1: (Color online) Separation of transport length scales in quantum Hall superfluid transport. This theory is intended to apply when the ordered state is well established and Hall angles are large because of the developing $\nu = 1$ quantum Hall effect. At large Hall angles current enters and leaves the samples at the *hot spot* corners, even when the source and drain contacts (gray) fully cover the ends of a Hall bar. When order is well established, the pseudospin orientation of the transport electrons achieves alignment with the condensate within a relatively small fraction of the sample area close to source and drain (solid yellow). In these areas pseudospin transfer torques convert transport currents into condensate counterflow supercurrents. When source and drain are connected to opposite layers a net supercurrent is injected into the interior region of the sample. In the remaining sample area (shaded blue) collective interlayer tunneling can act as a sink for the counterflow supercurrent.

antisymmetric or counterflow) fermionic pseudospin current. The last contribution would be viewed as a spin-transfer torque in the analogous equations for an easy-plane anisotropy ferromagnetic metal.

We start our qualitative discussion of critical currents by identifying some relevant length scales. First the length scale,

$$\lambda = \sqrt{\frac{2\rho_s}{\Delta_t n}}, \quad (8)$$

often referred to as the Josephson length because of the similarity between these equations and those which describe Josephson junctions, emerges from balancing the first and second terms. In this paper we assume that the pseudospin magnetization direction departs from the $\hat{x}-\hat{y}$ plane only over a small region close to the source and drain contacts whose spatial extent is small compared to the Josephson length. (This issue is addressed again in the discussion section.) If this is correct, we can separate length scales by identifying a region close to the contact which is small enough that we can ignore coherent tunneling by setting $\Delta_t n$ to 0, and large enough that we can assume that m_z is close to zero in the rest of the system. (See Fig. (1).) When $\Delta_t n \rightarrow 0$, Eq.(7) simply expresses the conservation of the sum of the excitonic and quasiparticle counterflow currents. Integration of Eq.(7) over the area close to the contact then simply describes con-

version of quasiparticle counterflow current into condensate counterflow current. The total counterflow current emerging from the area near the source contact is half of the total current flowing into the system since $m_z = \pm 1$ in the contact and $m_z \rightarrow 0$ far away from the contact. In a tunnel geometry experiment the same counterflow current is generated near the source and drain contacts located at opposite dies of the sample, so the total counterflow supercurrent injected *into* the system is equal to the total number current flowing *through* the system.

With this separation of length scales the quasiparticle (pseudospin transfer torque) term can be dropped in the remaining portion \tilde{A} of the total system area A . For static solutions of the LLS equations the condensate must satisfy an elliptic sine-Gordon equation inside \tilde{A} :

$$\lambda^2 \vec{\nabla}^2 \phi - \sin \phi = 0. \quad (9)$$

When $\lambda \rightarrow \infty$ ($\Delta_t n \rightarrow 0$), this equation states that $\vec{\nabla}^2 \phi$ is zero. It then follows from Green's theorem that no net counterflow supercurrent can flow into the area \tilde{A} . In the tunnel geometry that means that time-independent order parameter values cannot be maintained in the presence of a transport current unless $\Delta_t n \neq 0$. The maximum tunneling current that can flow through the system is particularly simple to determine in the small $\Delta_t n$, large λ limit. When λ is much larger than the system size the angle ϕ cannot vary substantially over the system area. With this simplification the elliptic sine-Gordon equation can be integrated over the area \tilde{A} to obtain

$$\rho_s \int_P \vec{\nabla} \phi \cdot \hat{n} = \frac{\rho_s \tilde{A}}{\lambda^2} \sin(\phi) \quad (10)$$

where P is the perimeter of \tilde{A} and \hat{n} is proportional to the outward normal. The left hand side of Eq.(10) is the net supercurrent which flows out of the region \tilde{A} from its boundaries near the source and drain contacts, identified above as the number current flowing through the system. Since the maximum value of $|\sin(\phi)|$ is 1, it follows that the maximum current consistent with a time-independent order parameter in this case is

$$I_B^c = \frac{e \tilde{A} \rho_s}{\hbar \lambda^2} = \frac{e \tilde{A} \Delta_t n}{2 \hbar}. \quad (11)$$

Since the critical current in the small $\Delta_t n$ limit is proportional to the area of the system we will refer to this quantity as the bulk critical current, as suggested by the notation used above.

For larger $\Delta_t n$, λ is no longer larger than the system size and it is not possible to maintain the maximum value of $\sin(\phi)$ across the system. The LLS equation critical current in this regime depends on geometric details and we have not been able to obtain rigorous bounds. We can make a rough estimate by following an argument along the following lines. The elliptic sine-Gordon equation is very similar to the regular sine-Gordon equation in which second order derivatives with respect to time and position

appear with opposite signs. This 1+1 dimensional sine-Gordon equation appears as the Euler-Lagrange equation of motion of a system with a Lagrangian with a kinetic-energy term proportional to $\rho_s(\partial_t\phi(x,t))^2$ and a potential energy term proportional $\Delta_t n \cos(\phi(x,t))$. Since total energy (integrated over position x) is conserved by this dynamics it follows that the variation of the typical value of $\rho_s(\partial_t\phi)^2$ along the space-time boundary cannot be larger than $\sim \Delta_t n$. When this energy conservation condition is mapped from the regular sine-Gordon equation to the (imaginary time) elliptic sine-Gordon equation we can conclude that the typical value of $\vec{\nabla}\phi \cdot \hat{n}$ along the boundary of \tilde{A} near the source contact cannot differ from the typical value of $\vec{\nabla}\phi \cdot \hat{n}$ along the boundary near the drain contact by more than $\sim \Delta_t n$. It follows that the current flowing through the system from source to drain should not be much larger than

$$I_E^c \sim \frac{eW\rho_s}{\hbar\lambda} \quad (12)$$

where W is the length of the contract region, or the width of a Hall bar assumed to be contacted at its edges. We will refer to I_E^c as the edge critical current, since it is limited by the length of one edge. For stronger inter-layer coupling then critical current is expected to vary as $(\Delta_t n)^{1/2}$ once λ is smaller than the Hall bar length. Finally we note that because of hot-spot effects in transport with large Hall angles the pseudospin transfer torque will act at the sample corners. Since the supercurrent is converted into coherent pseudospin precession over the length scale λ , the effective size of the contact region will be $\sim \lambda$ when the Hall angle is large and λ is smaller than W . We therefore estimate that the critical current is close to

$$I_C^c \sim \frac{e\rho_s}{\hbar}, \quad (13)$$

independent of $\Delta_t n$, under these circumstances. We refer to this last critical current as the corner critical current. In the following section we compare numerical LLS critical currents with these rough estimates.

IV. MODEL CALCULATIONS

The numerical calculations we describe below are similar to those carried out in micromagnetic descriptions of ferromagnetic metal spin-transfer torque physics, but are applied here to pseudospin transfer physics in condensed bilayers. We divide the system area into pixels within which the pseudospin magnetization is assumed to be constant. Except where noted we used square $10l \times 10l$ pixels where l is the magnetic length. We rewrite the spin-transfer torque term in Eq. (6) in the discretized form:

$$\dot{m}_\alpha|_{ST} = \sum_k \frac{I_n}{nA_{\text{pixel}}} [m_{k,\alpha} - (\vec{m}_k \cdot \vec{m})m_\alpha] \quad (14)$$

where k labels the four neighboring sites, A is the pixel area, and α labels components of the magnetization orientation in the pixel of interest. I_n is the quasiparticle number current flow from neighbor site n into this pixel. In this article we estimate values of I_n by solving the resistor network model obtained by discretizing a continuum model with a local conductivity that includes a Hall component.

$$\{I\} = [G]\{V\} \quad (15)$$

where $[G]$ is the conductance matrix that describes the local conductivity including Hall components, $\{V\}$ is a vector of local voltages in each pixel, and $\{I\}$ is a vector composed of currents that flow between pixels. Using current conservation conditions the dimension of the matrix can be reduced to the pixel number N . Given the source and drain contact voltages, we can solve for the internal voltage and current distributions and for the variation of source and drain currents across the contacts. Note that quantum Hall physics comes into play through the Hall contributions to the conductivity matrix $[G]$. The local Hall conductivity was set to $\sigma_{xy} = e^2/h$, which is close to the appropriate value for $\nu = 1$ whether or not the Hall plateau is fully formed, and the longitudinal conductivity was set to

$$\sigma_{xx} = 0.05 \exp(-m_z^2/W) (\vec{m} \cdot \vec{m}_L)(\vec{m} \cdot \vec{m}_R) e^2/h \quad (16)$$

where $\vec{m}_{L,R}$ is the magnetization orientation to the left and right of a boundary separating two-pixels. The Hall angle used in these calculations was therefore $\tan^{-1}(20)$ over the largest part of the sample in which the pseudospin magnetization is close to collinear and planar. The results we report on are not sensitive to the Hall angle, provided that it is large.

The current which flows into a pixel is assumed to have the same pseudospin polarization as the pixel from which it is incident. Currents entering or exiting from the contacts are assumed to have $m_z = 1$ for top layer contacts and $m_z = -1$ for bottom layer contacts. In this way the pseudospin transfer torque and the Landau-Lifshitz precessional torque acting on each pixel's pseudospin can be evaluated. Note that the pseudospin torque depends not only on current paths, but also on the pseudospin magnetization configuration.

A. Critical Current Identification

As mentioned in the previous section, we identify the critical current as the circuit current value above which a time independent solution no longer exists. When the external current is small, the Gilbert damping term in the LLS equation relaxes the pseudospin magnetization into time-independent configurations. The behavior of the pseudospin as the current increases is partly analogous to the behavior of a damped pendulum driven by an increasingly strong torque.

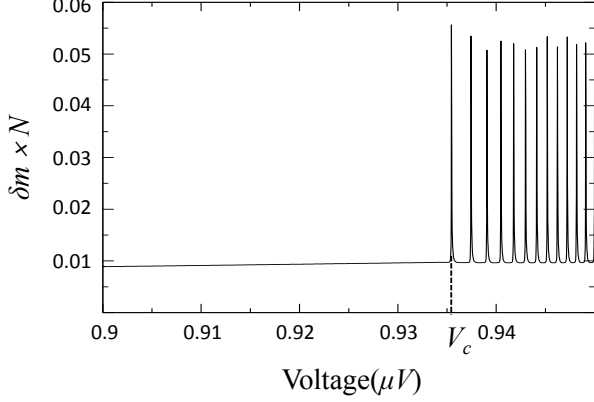


FIG. 2: Magnetization change per time step $\delta m \times N$ vs. applied voltage in a $500l \times 400l$ system for $2\pi l^2 n \Delta_t = 10^{-5} E_0$. This curve was obtained by changing the bias voltage by $\delta V = 2.5 \times 10^{-5} \mu V$ at each time step. $E_0 = e^2/\epsilon l$, the energy unit used in all our calculations has a typical experimental value ~ 7 meV. δm develops large amplitude oscillation when the voltage exceeds the critical voltage V_c .

We identify the critical current numerically by slowly increasing the driving voltage (by δV per time step) and monitoring the change in magnetization. To be more explicit, we examine

$$\delta m \equiv \sum_i |\vec{m}_i(V + \delta V) - \vec{m}_i(V)|/N \quad (17)$$

The sum in Eq.(17) is over all pixels. The critical current can be defined precisely as the current above which δm remains finite when $\delta V \rightarrow 0$. In practice we choose a suitably small value of δV and examine the current or voltage dependence of δm . We find that δm increases dramatically and begins oscillating at a voltage we identify as the critical voltage. (See Fig.(2).) An alternative but more laborious method of obtaining critical currents is to sequentially examine the dynamics of the pseudospin magnetization at a series of fixed values of the applied voltage V . If the applied voltage is below its critical value, δm will approach zero exponentially at large times. If the applied voltage is above its critical value δm will not approach zero and usually exhibits an oscillatory time dependence. In our calculations we used the first approach to determine an approximate value of the critical voltage (and hence the critical current) and the second method to refine accuracy.

B. I_c vs. Δ_t

It is useful to start by briefly discussing the single-pixel limit of the calculation, which should apply approximately to the case in which the Josephson length

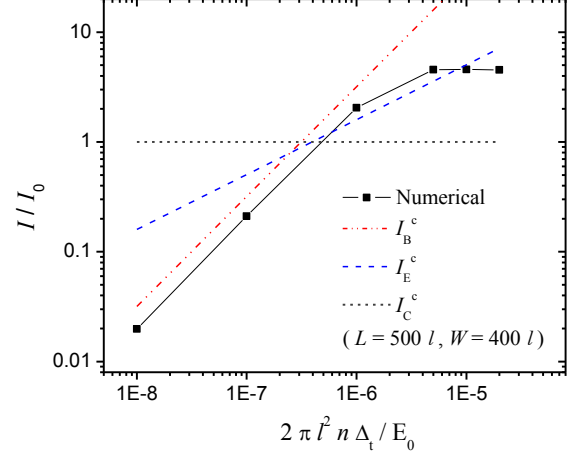


FIG. 3: (Color online) Critical current vs. $2\pi l^2 n \Delta_t$ in a $400l \times 500l$ system. The dash-dot (red), long-dash (blue) and short-dash (black) curves plot the values of the bulk (I_B^c), edge (I_E^c) and corner (I_C^c) limited critical currents discussed in the text for this sample geometry. The square dots plot LLS equation critical currents at a series of $\Delta_t n$ values. All the calculations in this paper were performed using pseudospin stiffness (exciton superfluid density) $\rho_s = 0.005 E_0$ where $E_0 = e^2/\epsilon l$ is the energy unit. Currents are in units of $I_0 = I_E^c = e\rho_s/\hbar$. For the value of ρ_s used in these calculations $I_0 \simeq 8nA$.

is longer than the system size. The steady limit of the LLS equation for the \hat{z} -component of the pseudospin is

$$0 = \frac{1}{2} \frac{\Delta_t n A_{\text{pixel}}}{\hbar} \sin \phi - \frac{I}{2e} (m_{z,L} - m_{z,R}) \quad (18)$$

where I is the charge current flowing through the system and $m_{z,L}$ and $m_{z,R}$ are the z component of pseudospin for the source and drain leads at the left and right ends of the sample. For the drag geometry (current entering and exiting from the same layer) $m_{z,L} = m_{z,R}$, there is no spin torque term in the single-pixel calculation, and the steady state equation can be satisfied by setting $\sin \phi = 0$. For the tunneling geometry $m_{z,L} = -m_{z,R}$, the maximum pseudospin torque that can be compensated by the tunneling term is obtained by setting $\sin \phi \rightarrow 1$. We therefore obtain

$$I^c = I_B^c = \frac{e}{2\hbar} \Delta_t n A_{\text{pixel}} \quad (19)$$

This gives a linear dependence of I_c on the single-particle tunneling strength Δ_t . The numerical procedures described above accurately reproduce this simple result.

As explained previously and discussed more fully later, we believe that the pseudospin transfer torque in most quantum Hall superfluid experiments acts in a small fraction of the system area. We therefore need to perform calculations with many pixels in order to represent a typical measurement. Fig. (3) shows numerical critical current results for a fixed sample geometry as a function of

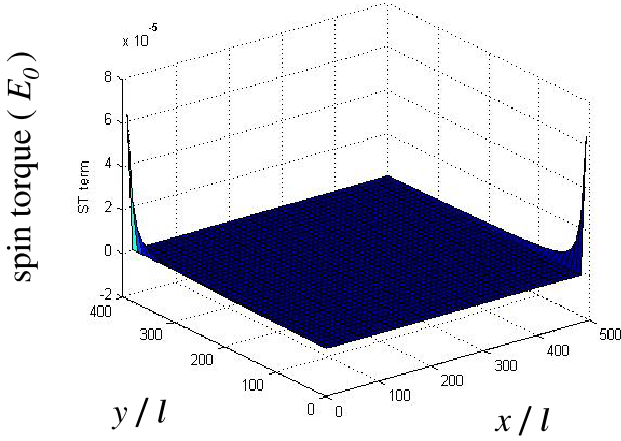


FIG. 4: Spatial distribution of the \hat{z} component of the pseudospin transfer torque in a system with $500 \times 400 l^2$ area, $2\pi l^2 n \Delta_t = 10^{-6} E_0$, and $I/I^c = 0.29$. The pseudospin transfer torque in the model studied here acts mainly in the hot spot pixels. E_0 and l are defined as in previous figures.

Δ_t . In this figure $I_0 = I_C^c = e\rho_s/\hbar \sim 8nA$ is the unit of current and $E_0 = e^2/\epsilon l$ is the unit of energy. Typical quantum Hall superfluid experiments are performed at a magnetic field of roughly 2.1 Tesla for which the magnetic length is 17.65 nm which gives $E_0 = 6.4$ meV. In all the calculations reported on here we used a pixel area $A_{\text{pixel}} = 10 \times 10 l^2$ and the mean-field theory estimate⁷ ($\rho_s \simeq 0.005 E_0$) for the pseudospin stiffness. The calculations in Fig.(3) are for 40 pixels in the width W direction and 50 pixels in the current L direction. For this system size, the Josephson length is approximately equal to L when $2\pi l^2 \Delta_t n \sim 4 \times 10^{-7} E_0$. The numerical results illustrated in Fig. (3) show the crossovers from Δ_t -dependence, to $\Delta_t^{1/2}$ -dependence, to saturation as Δ_t increases that was anticipated in our qualitative discussion. At small $\Delta_t n$ the critical current is reduced by a small fraction compared to the single pixel result in accord with the Fig.(1).

We now examine the ingredients which enter these numerical results in greater detail. According to the schematic Fig. (1), the pseudospin transfer torque acts only near the hot spots at which current enters and exits the sample. Fig. (4) shows a typical numerical results for the spatial distribution of the pseudospin transfer torque. In the present model, the area of the region in which transport current is converted into supercurrent depends on the pixel size and the pseudospin stiffness and anisotropy coefficients. In the tunneling geometry, counterflow supercurrent is generated near both source and drain hot spots and flows diagonally toward the center of the sample. In Fig. (5) we show a typical supercurrent distribution for the tunneling geometry case. The corresponding distribution for an equivalent drag experiment (both contacts connected to the same layer) is illustrated in Fig. (6). Since the elliptic sine-Gordon

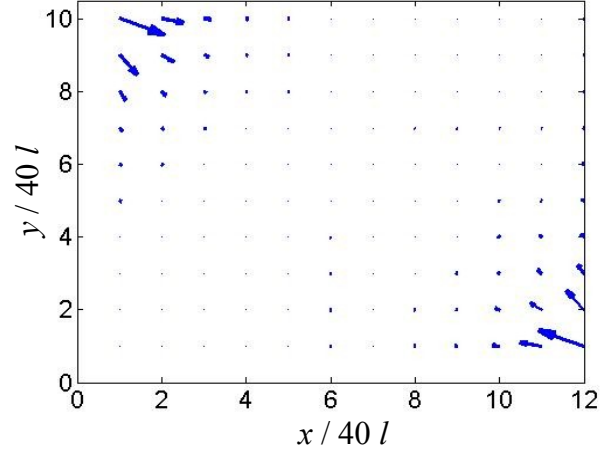


FIG. 5: Supercurrent distribution in system with area $500 \times 400 l^2$, $2\pi l^2 n \Delta_t = 10^{-6} E_0$, and $I/I^c = 0.29$. This plot is for a tunneling geometry in which the source is a top layer contact and the drain is a bottom layer contact. Supercurrents are generated near both hot spots and flow diagonally toward the sample center. E_0 and l are defined as in previous figures.

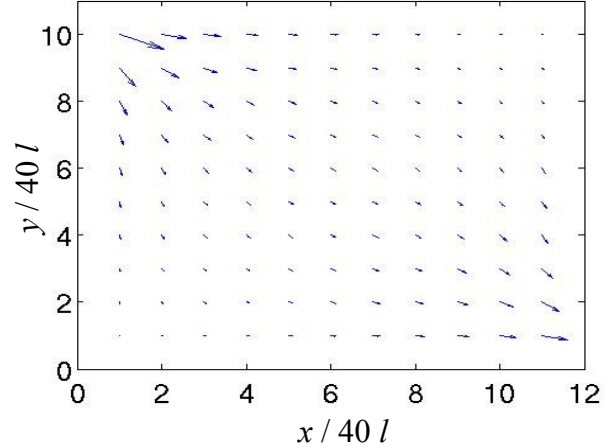


FIG. 6: Supercurrent distribution in system with area $500 \times 400 l^2$, $2\pi l^2 n \Delta_t = 10^{-6} E_0$. This plot is for the drag geometry case in which the source and drain are both top layer contacts, but other parameters of the calculation are identical to those used in the preceding tunnel-geometry figure. E_0 and l are defined as in previous figures.

equation applies locally when the pseudospin transfer torque is negligible, it follows from Green's theorem and Eq.(7) that in a steady state the total counterflow current injected into the interior of the sample (which for the tunnel geometry equals the total charge current flowing through the system) must match the area integration of $(1/2)(\Delta_t n/\hbar) \sin \phi$. For a drag geometry experiment the same integral should vanish.

We now examine steady state condensate configurations at currents near the critical current for both small

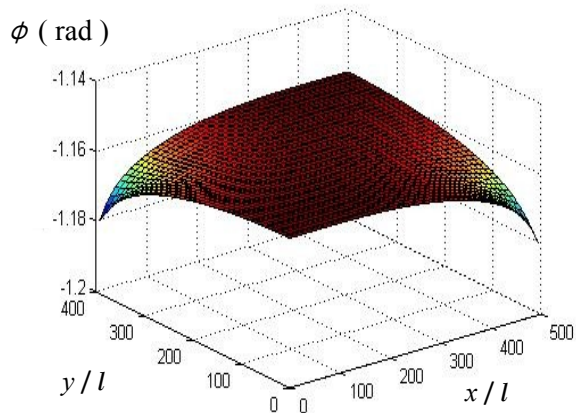


FIG. 7: Pseudospin phase distribution in a system with area $500 \times 400 l^2$, $2\pi l^2 n \Delta_t = 10^{-8} E_0$ and $I/I^c = 0.75$. The Josephson length at this value of Δ_t is $\sim 2500l$. Note that ϕ is roughly constant through the system and that its value is close to $\pi/2$ because I is close to I_c . The units used here are the same as in previous figures.

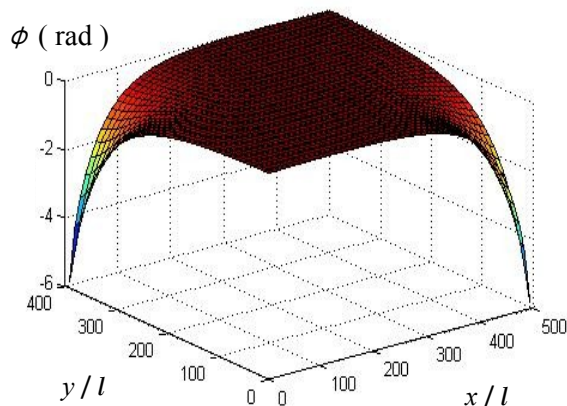


FIG. 8: Phase distribution of pseudospin in a system with area $500 \times 400 l^2$, $2\pi l^2 n \Delta_t = 1.2 \times 10^{-5} E_0$ and $I/I^c = 0.97$. The Josephson length at this value of Δ_t is $\sim 70l$. Note that a steady state is reached even though ϕ varies considerably across the sample and has values larger than $\pi/2$. The units used here are the same as in previous figures.

$n\Delta_t$ and large $n\Delta_t$ limits. In the former case our expectation that $\sin \phi$ should be nearly constant except near the hot spots is confirmed in Fig. (7). Collective tunneling acts sinks the injected counterflow supercurrent at a rate that is nearly constant across the sample area. The large $n\Delta_t$ case is more complex. ϕ varies over a large range and $\sin(\phi)$ changes sign in different parts of the sample. Near the sample corners ϕ varies rapidly with position because of the large counterflow supercurrents. In the interior of the sample the phase changes less rapidly because the

flow pattern spreads and because coherent tunneling is providing the required current sink. The critical current in the large $n\Delta_t$ limit, depends in a complex way on the geometry of the sample and on the spatial distribution of the pseudospin transfer torques. Nevertheless, the critical current saturation we find in our numerical studies suggests that once the Josephson length is smaller compared to both the width and the length of a Hall bar sample with a large Hall angle, it is no longer relevant to the critical current value.

C. I_c vs. System Geometry

Finally, we briefly discuss critical current dependence on Hall bar dimensions at fixed $n\Delta_t$. In Fig.(9) we plot I^c vs. Hall bar length in a series of model samples with a fixed single pixel width $W = 10l$ and single-particle tunneling amplitude $2\pi l^2 n \Delta_t = 10^{-6} E_0$. For these parameters the W is much smaller than the Josephson length. The critical current increases linearly with sample length and is therefore proportional to sample area until it saturates at $L \sim 1000l$. The length at which the current saturates is a bit longer than the Josephson length and the value of the critical current is accordingly somewhat larger than the 1D estimate²¹ I_E^c . The large L behavior is however consistent with the expectation that the critical current should not increase with system length once L is substantially larger than the Josephson length λ . In Fig. (10) we plot I_c vs. system width W with the length fixed at $500l$ and the same Δ_t as above. The range of W covered is limited somewhat by numerical practicalities and goes from a width much smaller than the Josephson length to a width which is somewhat larger. Over this range deviations from the 1D model in which the critical current is proportional to Hall bar width are small.

V. DISCUSSION AND CONCLUSIONS

We start our discussion by commenting briefly on some essential differences between the critical current of a Josephson junction and critical currents for coherent bilayer tunneling. In a Josephson junction, current can flow without dissipation across a thin insulating layer that separates two superconductors. The difference in condensate phase across the junction ϕ_J is normally zero in equilibrium but can be driven to a non-zero steady state value when biased by current flow I_J in the circuit in which the junction is placed. For thick insulating layers the current is related to the phase difference by

$$I_J = I_J^c \sin(\phi_J), \quad (20)$$

where I_J^c is the junction's critical current. Eq.(20) should be compared with Eq.(7). The most obvious difference is the appearance of the lateral 2D coordinate in the coherent bilayer case. In the Josephson junction case, the

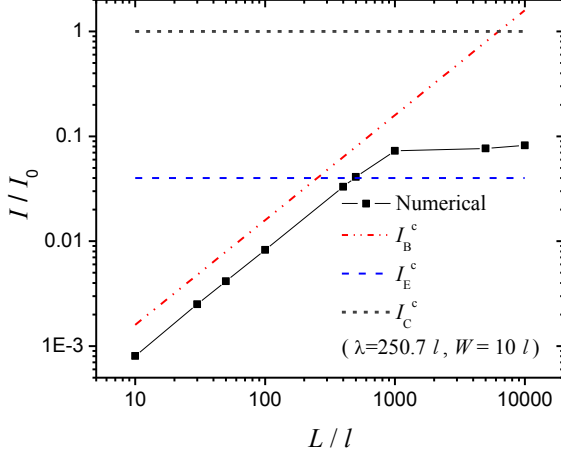


FIG. 9: Critical current *vs.* system length L for a narrow Hall bar with width $W = 10 l$. The single-particle tunneling amplitude $2\pi l^2 n \Delta_t = 10^{-6}(E_0)$ corresponding to $\lambda \sim 250l$

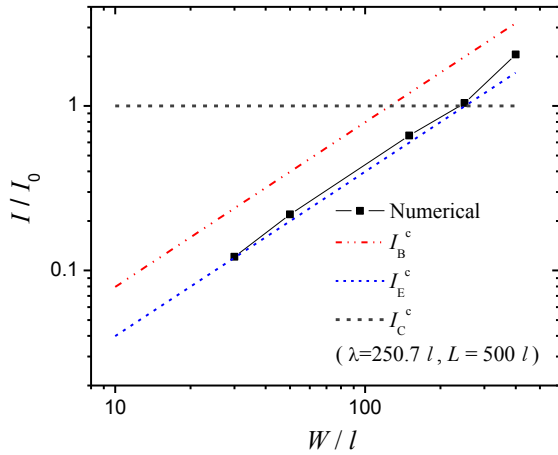


FIG. 10: Critical current *v.s.* system width W for length $L = 500 l$. The single-particle tunneling amplitude $2\pi l^2 n \Delta_t = 10^{-6}(E_0)$, corresponding to $\lambda \sim 250l$

lateral dependence of ϕ_J usually plays no role unless an external magnetic field is present. In the coherent bilayer case, on the other hand, lateral translational invariance is always broken because the pseudospin transfer torques that ultimately drive the coherent tunneling current do not act uniformly across the system.

A closer comparison is possible in the special case in which the pseudospin stiffness is large enough to inhibit lateral variation of ϕ . Integration of Eq. (7) over the area then yields for the coherent bilayer

$$I_{BL} = I_B^c \sin(\phi) \quad (21)$$

where I_B^c is the bulk critical current discussed in the body

of the paper and

$$I_{BL} = e \int_P \left[\frac{\rho_s}{\hbar} \vec{\nabla} \phi + \frac{m_z}{2} \vec{j} m_z \right] \cdot \hat{n}. \quad (22)$$

is the injected counterflow current. The most essential difference between tunneling in coherent quantum Hall bilayers and Josephson junctions lies in the difference in physical content between the bias currents I_J and I_{BL} . In the case of a Josephson junction it is a bulk dissipationless supercurrent which flows perpendicular to the plane of the junction. In the case of a coherent quantum Hall bilayer, it is the counterflow (\hat{z}) component of the quasiparticle current. The counterflow component of the quasiparticle current is normally fully converted to condensate counterflow supercurrents by pseudospin transfer torques, as we have discussed at length. The voltage drop across a Josephson junction can be measured and vanishes below the critical current. Because fermionic quasiparticle transport, transverse counterflow supercurrents, and collective interlayer tunneling are unavoidably intertwined in the coherent bilayer tunneling case, there is no corresponding measurable voltage which vanishes below the critical current. Instead, the critical current is marked experimentally by an abrupt increase in measured resistances.

Next we draw attention to the significance of the qualitative difference in experiment between drag geometry and tunnel geometry transport measurements. In our theoretical picture is correct there should be no qualitative difference between voltage measurements in these two geometries at currents below the critical current, once coherence is well established. (Important differences between these measuring geometries can occur in the interesting regime close to the phase boundary where interlayer coherence may be established over a small fraction of the sample area.³⁴) Pseudospin transfer torques in tunnel and drag geometry experiments with similar total circuit currents give rise to similar counterflow supercurrents, as seen in Figs. (5) and (6). Excitonic condensates have a maximum local (critical) supercurrent density that they can support, which in the case of quantum Hall bilayer exciton condensates has been estimated³⁵ to be $\sim 1 \text{ Am}^{-1}$. For a typical sample width of 10^{-4} m this corresponds to a critical current in the mA regime, orders of magnitude larger than the current levels typically employed in quantum Hall experiments. Even accounting for possible corrections due to disorder, local critical currents are unlikely to be approached experimentally for either contact geometry. (If they were, we would expect more similarity between the two experiments.) The critical currents which are important for typical tunneling experiments are not local critical currents, but global critical currents which set an upper limit on the rate at which injected supercurrent can be sunk by collective tunneling. Since there is no net injected supercurrent in the drag geometry experiment, only local limits apply. In the tunnel-geometry experiment, the global limit must be satisfied, setting a critical current scale which can be

orders of magnitude smaller if Δ_t is small. Although the relationship anticipated here between tunneling geometry and drag geometry transport has not been specifically tested experimentally, it appears to us that it is clearly consistent with published data.

We now turn to a comparison of our theory with experiment, and in particular with the recent experiments of Tiemann *et al.*³² who have systematically studied the dependence of the tunneling critical currents in their samples on temperature and layer separation. The data of Tiemann *et al.* appear to be broadly consistent with that reported in earlier^{8,16} but focus more on tunneling anomalies in the region of the phase diagram far from the coherent state phase boundary. Tiemann *et al.* find i) that the critical tunneling currents in their samples are proportional to system area, ii) that their typical value is $\sim 10\text{nA mm}^{-2}$, and that they saturate upon moving away from the coherent state phase boundary²⁷ either by lowering temperature or by decreasing the ratio of layer separation to magnetic length.

Tiemann *et al.*'s finding that the critical current is proportional to area would be consistent with our analysis if the Josephson length was comparable to or longer than the $\sim 10\text{mm}$ length of their long-thin Hall bars. When in the bulk-limited critical current regime, the critical current should be given by I_B^c

$$\frac{I_B^c}{A} = \frac{e\tilde{\Delta}_t}{4\pi l^2 \hbar} = 3.1B[\text{Tesla}] \times \tilde{\Delta}_t[\text{eV}] \times 10^4 \text{A mm}^{-2} \quad (23)$$

where $\tilde{\Delta}_t = 2\pi l^2 \Delta_t n$ is the interlayer tunneling amplitude suitably renormalized by quantum and thermal fluctuations and B is the magnetic field strength at $\nu = 1$. Inserting the magnetic field strength, experimental critical currents can be recovered by setting $\tilde{\Delta}_t \rightarrow 10^{-13}\text{eV}$. Therein lies the rub. Although values for $\tilde{\Delta}_t$ on this scale do imply Josephson lengths that are on the mm length scale and therefore consistent with bulk-limited critical currents in the samples studied by Tiemann *et al.*, they are four or more orders of magnitude smaller than values expected on the basis of theoretical estimates. Suspicion that there is a fundamental discrepancy is established more convincingly, perhaps, by observing that these critical currents also correspond to $\tilde{\Delta}_t$ values several orders of magnitude smaller than seemingly reliable experimental estimates³³ based on the inter-layer tunneling conductance in similar samples at zero-field. The key issue then in comparing critical current theories with experiment appears to be explaining why they are so small.

We expect on general grounds that the experimental value of $\Delta_t n \equiv \Delta_t/2\pi l^2$ should be renormalized downward by both thermal and quantum fluctuations and by disorder. Indeed according to the familiar Mermin-Wagner theorem, the order parameter n must vanish for $\Delta_t \rightarrow 0$ at finite temperatures. The importance of thermal fluctuations is strongly influenced by $k_B T/\rho_s$. If mean-field theory estimates⁷ of ρ_s can be trusted, the value of ρ_s in typical experimental samples should be $\sim 3 \times 10^{-5}\text{eV}$ and $k_B T/\rho_s$ should therefore be less than

0.1 at the lowest measurement temperatures. At these low temperatures thermal fluctuations alone appear to be insufficient³⁶ to explain the discrepancy even though $\Delta_t/k_B T$ is certainly small. The experimental finding that the critical current saturates at low temperatures supports this conclusion. Similarly, theoretical estimates that quantum fluctuation corrections to the order parameter are not²⁵ large well away from the transition boundary are consistent with the experimental finding of saturating critical currents in this regime. It appears that an explanation for the small critical currents must be found in the disorder physics of quantum Hall superfluids.

The analysis of tunneling critical currents presented in this paper can accommodate disorder implicitly through its influence on the parameters ρ_s and $\Delta_t n$. Including disorder effects through renormalized coupling constants would be adequate if the characteristic length scales for disorder physics are smaller than characteristic length scales like λ which are relevant for pseudospin transfer torques. In quantum Hall superfluids disorder may play a more essential role by nucleating charged merons³⁷ (vortices). As we have explained, provided that the pseudospin transfer torque acts only close to the source and drain, the critical current is proportional to the integral of $\Delta_t n$ over the area of the sample. This integral is reduced to zero by a single undistorted meron located at the center of a large sample. It has in fact often^{12-14,40-42} been recognized that disorder induced vortices might play an essential role in many of the transport anomalies associated with bilayer coherence. It seems likely to us that this type of physics is very likely responsible for the small critical currents seen in experiment, but that existing theory is unable to account for this effect quantitatively. The current status of the subject calls for a detailed analysis of how they influence critical currents. On the experimental side, the importance of complex disorder-related pseudospin textures for critical current values could be reduced and the essential physics which limits critical currents revealed more clearly by studying samples with much larger bare values of Δ_t .

Although we have attributed the substantial quantitative disagreement between pseudospin transfer torque theory and experiment to disorder-induced pseudospin textures and have suggested a strategy for achieving more quantitative tests of our theory, it is appropriate to step-back and reconsider other theoretical pictures that might be relevant to coherent bilayer tunneling experiments under some circumstances. For example, the version of the pseudospin-transfer torque theory applied here is based on the simplest possible assumption for the local pseudospin-polarization of the transport current, namely that the pseudospin current polarization simply follows the pseudospin density polarization. This assumption is certainly not generically correct, but its replacement requires more detailed knowledge of fermionic quasiparticle transport behavior. One approach is to assume that the quantum Hall effect establishes edge state transport and use experimental voltage probe data to infer³⁸ the

length scale on which the pseudospin polarization of injected electrons is relaxed, and therefore the length scale over which the pseudospin transfer torque acts. The advantage of this approach is that experimental data could be used to obtain the spatial distribution of pseudospin transfer torques. Examination of coherent bilayer transport data suggests³⁹ that the torques sometimes act along most of the perimeter of the system, as assumed in a previous¹⁸ attempt to understand coherent-bilayer tunneling data, and sometimes close to the source and drain the contacts as assumed here. The current model is most appropriate well away from the coherent state phase boundary as we have discussed.

The present version of the pseudospin transport torque theory does not account for thermal or quantum fluctuations of the condensate, which are unimportant in metallic ferromagnets but might sometimes be important in coherent bilayers. Weak-coupling theories^{12–15} of bilayer tunneling do account for fluctuations, but treat Δ_t per-

turbatively. These theories cannot account for the existence of a critical currents and in practice assume that each layer has a separate well-defined local chemical potential. It is clear from published transport data that this assumption is not always valid, in particular that it is not valid in the portion of the phase diagram far away from the phase boundary on which the present paper focuses. Experimentally³² the critical current value decreases as the phase boundary of the coherent state is approached by increasing either temperature or the effective layer separation d/l . It would be interesting to attempt quantitative tests of the predictions of weak-coupling theories in the portion of the phase diagram close to the phase boundary.

The authors acknowledge essential contributions by T. Pereg-Barnea to initial stages of this work and insights gained from valuable discussions with A. Balatsky, J.P. Eisenstein, W. Dietsche, A.D.K. Finck, Y. Joglekar, D. Pesin, L. Radzihovsky, L. Tiemann, and K. von Klitzing.

-
- ¹ H. A. Fertig, Phys. Rev. B **40**, 1087 (1989).
 - ² A. H. MacDonald, P. M. Platzman, and G. S. Boebinger, Phys. Rev. Lett. **65**, 775 (1990).
 - ³ X.-G. Wen and A. Zee, Phys. Rev. Lett. **69**, 1811 (1992).
 - ⁴ J. P. Eisenstein and A. H. MacDonald, Nature **432**, 691 (2004).
 - ⁵ A. H. MacDonald, E. H. Rezayi, Phys. Rev. B **42**, 3224 (1990).
 - ⁶ A. H. MacDonald, Physica B **298**, 129 (2001).
 - ⁷ K. Moon, H. Mori, Kun Yang, S. M. Girvin, A. H. MacDonald, L. Zheng, D. Yoshioka, and Shou-Cheng Zhang, Phys. Rev. B **51**, 5138 (1995).
 - ⁸ I. B. Spielman, J. P. Eisenstein, L. N. Pfeiffer, and K. W. West, Phys. Rev. Lett. **84**, 5808 (2000).
 - ⁹ I. B. Spielman, M. Kellogg, J. P. Eisenstein, L. N. Pfeiffer, and K. W. West, Phys. Rev. B **70**, 081303(R) (2004); A. D. K. Finck, A. R. Champagne, J. P. Eisenstein, L. N. Pfeiffer, and K. W. West, Phys. Rev. B **78**, 075302 (2008).
 - ¹⁰ E. Tutuc, S. Melinte, E. P. De Poortere, R. Pillarisetty, and M. Shayegan, Phys. Rev. Lett. **91**, 076802 (2003); E. Tutuc, M. Shayegan and D. A. Huse, Phys. Rev. Lett. **93**, 036802 (2004).
 - ¹¹ R. D. Wiersma, J. G. S. Lok, S. Kraus, W. Dietsche, K. von Klitzing, D. Schuh, M. Bichler, H. P. Tranitz, and W. Wegscheider, Phys. Rev. Lett. **93**, 266805 (2004); L. Tiemann, J. G. S. Lok, W. Dietsche, K. von Klitzing, K. Muraki, D. Schuh, and W. Wegscheider, Phys. Rev. B **77**, 033306 (2008).
 - ¹² A. Stern, S.M. Girvin, A. H. MacDonald, and Ning Ma, Phys. Rev. Lett. **86**, 1829 (2001).
 - ¹³ L. Balents and L. Radzihovsky, Phys. Rev. Lett. **86**, 1825 (2001).
 - ¹⁴ M. M. Fogler and F. Wilczek, Phys. Rev. Lett. **86**, 1833 (2001).
 - ¹⁵ R. L. Jack, D. K. K. Lee, and N. R. Cooper, Phys. Rev. Lett. **93**, 126803 (2004), *ibid* Phys. Rev. B **71**, 085310 (2005); O. G. C. Ros and D. K. K. Lee, arXiv:0911.2647.
 - ¹⁶ I. B. Spielman, J. P. Eisenstein, L. N. Pfeiffer, and K. W. West, Phys. Rev. Lett. **87**, 036803 (2001). Instead of splitting the zero-bias conductance peak into two finite-bias peaks, a parallel field gradually decreases its height. Small features appear in the tails of these peaks near the voltages at which the conductance peaks are expected in the weak-coupling theory.
 - ¹⁷ X. G. Wen and A. Zee, Phys. Rev. B **47**, 2265 (1993).
 - ¹⁸ E. Rossi, A. S. Nunez, and A. H. MacDonald, Phys. Rev. Lett. **95**, 266804 (2005).
 - ¹⁹ R. Khomeriki, L. Tkeshelashvili, T. Buishvili, and Sh. Revishvili, Eur. Phys. J. B **51**, 421 (2006).
 - ²⁰ D. V. Fil and S. I. Shevchenko, J. Low Temp Phys. **33**, 780 (2007).
 - ²¹ J.-J. Su, and A. H. MacDonald, Nature Physics **4**, 799 (2008).
 - ²² See D. C. Ralph, and M. D. Stiles, J. Magn. Mag. Mater. **320**, 1190 (2008) and work cited therein.
 - ²³ J. C. Slonczewski, J. Magn. Magn. Mater. **159**, L1 (1996).
 - ²⁴ A. A. Burkov and A. H. MacDonald, Phys. Rev. B **66**, 115320 (2002).
 - ²⁵ Y. N. Joglekar and A. H. MacDonald, Phys. Rev. B **64**, 155315 (2001).
 - ²⁶ Y. N. Joglekar and A. H. MacDonald, Phys. Rev. Lett. **87**, 196802 (2001). The analysis of tunneling transport in this paper is incomplete because of the absence of a pseudospin transfer torque term in the condensate equations of motion.
 - ²⁷ A. R. Champagne, J. P. Eisenstein, L. N. Pfeiffer, and K. W. West, Phys. Rev. Lett. **100**, 096801 (2008); P. Giudici, K. Muraki, N. Kumada, Y. Hirayama, and T. Fujisawa, Phys. Rev. Lett. **100**, 106803 (2008); A. D. K. Finck, J. P. Eisenstein, L. N. Pfeiffer, K. W. West, arXiv:0911.2461.
 - ²⁸ Strictly speaking the statements are true only if the potential terms in the Schrodinger equation are local, a property not satisfied by exchange potentials. This limitation is irrelevant since our goal is to describe systems with pseudospin textures that are smooth on microscopic length scales.
 - ²⁹ A. S. Nunez and A. H. MacDonald, Solid State Comm., **139**, 31 (2006).
 - ³⁰ See for example P. M. Haney, R. A. Duine, A. S. Nunez, and A. H. MacDonald, J. Magn. Mag. Mater. **320**, 1300

- (2008).
- ³¹ A. R. Champagne, A. D. K. Finck, J. P. Eisenstein, L. N. Pfeiffer, and K. W. West, Phys. Rev. B **78**, 205310 (2008).
 - ³² L. Tiemann, Y. Yoon, W. Dietsche, K. von Klitzing, and W. Wegscheider, Phys. Rev. B **80**, 165120 (2009).
 - ³³ I. B. Spielman, Ph.D. Thesis, California Institute of Technology (2004).
 - ³⁴ A. Stern and B. I. Halperin, Phys. Rev. Lett. **88**, 106801 (2002).
 - ³⁵ M. Abolfath, A. H. MacDonald, and L. Radzihovsky, Phys. Rev. B **68**, 155318 (2003).
 - ³⁶ D. Pesin and A. H. MacDonald, in preparation.
 - ³⁷ S. Q. Murphy, J. P. Eisenstein, G. S. Boebinger, L. N. Pfeiffer, and K. W. West, Phys. Rev. Lett. **72**, 728 (1994).
 - ³⁸ D. Yoshioka and A. H. MacDonald, Phys. Rev. B **53**, R16168 (1996).
 - ³⁹ J. P. Eisenstein and A. H. MacDonald, unpublished.
 - ⁴⁰ P. R. Eastham, N. R. Cooper and D. K. K. Lee, Phys. Rev. B **80**, 045302 (2009).
 - ⁴¹ H. A. Fertig and G. Murthy, Phys. Rev. Lett. **95**, 156802 (2005).
 - ⁴² B. Roostaei, K. J. Mullen, H. A. Fertig, and S. H. Simon, Phys. Rev. Lett. **101**, 046804 (2008).